doi:10.1093/jmcb/mjv066
Published online December 28, 2015

Article

IRE1–RACK1 axis orchestrates ER stress preconditioning-elicited cytoprotection from ischemia/reperfusion injury in liver

Dong Liu[1,7,†], Xing Liu[2,†], Ti Zhou[1], William Yao[3], Jun Zhao[4], Zhigang Zheng[1], Wei Jiang[1], Fengsong Wang[2,3,5], Felix O. Aikhionbare[3], Donald L. Hill[6], Nerimah Emmett[3], Zhen Guo[2], Dongmei Wang[2], Xuebiao Yao[3,*], and Yong Chen[1,*]

[1] Department of Hepatobiliary Surgery, Xijing Hospital, Fourth Military Medical University, Xi'an 710032, China
[2] Anhui Key Laboratory of Cellular Dynamics and Hefei National Laboratory for Physical Sciences at Nanoscale, Hefei 230027, China
[3] Atlanta Clinical & Translational Science Institute, Atlanta, GA 30310, USA
[4] Department of Pathology, Xijing Hospital, Fourth Military Medical University, Xi'an 710032, China
[5] Department of Biochemistry, Anhui Medical University, Hefei 230027, China
[6] Comprehensive Cancer Center, University of Alabama at Birmingham, Birmingham, AL 35294, USA
[7] Present address: Department of Hepatobiliary Surgery, Navy General Hospital, Beijing 100048, China
[†] These authors contributed equally to this work.
[*] Correspondence to: Yong Chen, E-mail: yongchen62@yahoo.com; Xuebiao Yao, E-mail: xyao@msm.edu

Endoplasmic reticulum (ER) stress is involved in ischemic preconditioning that protects various organs from ischemia/reperfusion (I/R) injury. We established an *in vivo* ER stress preconditioning model in which tunicamycin was injected into rats before hepatic I/R. The hepatic I/R injury, demonstrated by serum aminotransferase level and the ultra-structure of the liver, was alleviated by administration of tunicamycin, which induced ER stress in rat liver by activating inositol-requiring enzyme 1 (IRE1) and upregulating 78 kDa glucose-regulated protein (GRP78). The proteomic identification for IRE1 binders revealed interaction and cooperation among receptor for activated C kinase 1 (RACK1), phosphorylated AMPK, and IRE1 under ER stress conditions in a spatiotemporal manner. Furthermore, *in vitro* ER stress preconditioning was induced by thapsigargin and tunicamycin in L02 and HepG2 cells. Surprisingly, BCL2 was found to be phosphorylated by IRE1 under ER stress conditions to prevent apoptotic process by activation of autophagy. In conclusion, ER stress preconditioning protects against hepatic I/R injury, which is orchestrated by IRE1–RACK1 axis through the activation of BCL2. Our findings provide novel insights into the molecular pathways underlying ER stress preconditioning-elicited cytoprotective effect against hepatic I/R injury.

Keywords: IRE1, RACK1, AMPK, BCL2, ER stress preconditioning, ischemia/reperfusion injury

Introduction

Endoplasmic reticulum (ER) stress is involved in various chronic and acute pathological conditions, including type 2 diabetes, and cancer as well as in ischemia/reperfusion (I/R) injury (Harding et al., 1999). It is marked by the accumulation, in the ER lumen, of unfolded or misfolded proteins, which elicits a wide range of signaling pathways through three ER membrane resident proteins inositol-requiring kinase 1 (IRE1), protein kinase RNA-like endoplasmic reticulum kinase (PERK), and activating transcription factor 6 (ATF6). ER stress results in shutdown of protein translation and over-expression of molecular chaperones such as 78 kDa glucose-regulated protein (GRP78; Schroder and Kaufman, 2005). These stress responses promote cell survival, and are altogether called the unfolded protein response (UPR; Ron and Walter, 2007). Generally, stresses leading to the accumulation of misfolded proteins in the ER lumen cause the disassociation of binding GRP78, from the luminal regions of the transmembrane proteins and thereby lead to their activation (Shen et al., 2002). With a cytoplasmic region consisting of a phosphorylation and an endonuclease domain, IRE1 activates itself by homo-dimerization in the luminal region and by auto-phosphorylation in the cytoplasmic region (Machamer et al., 1990). The endonuclease domain activates the transcription factor XBP-1 (X-box binding protein) pre-mRNA by cleavage and removal of a 26-bp intron (Calfon et al., 2002). This activated transcription factor binds to stress element promoters in the nucleus and upregulates the UPR stress genes, including that for GRP78 (McCullough et al., 2001). However, persistent ER stress is harmful as it provokes programmed cell death (Wang et al., 1998; Nakagawa et al., 2000).

Received January 18, 2015. Revised September 8, 2015. Accepted September 22, 2015.

Ischemic preconditioning (IPC) efficiently alleviates I/R injury to the heart, kidneys, lungs, liver (Carini and Albano, 2003), and other organs (Malhi and Gores, 2008). Short intervals of I/R provide protection against subsequent severe I/R injury (Murry et al., 1991). The mechanism associated with this protective effect has not been defined (Eisen et al., 2004). GRP78 over-expression is involved in the protective effect of IPC against delayed neuronal cell death (DND) caused by ischemia (Hayashi et al., 2003), suggesting a role for ER stress in IPC. ER stress is attenuated by IPC, which could be the basis for less DND after ischemia. Further, by reducing oxidative and ER stress, early IPC protects kidneys against I/R injury (Mahfoudh-Boussaid et al., 2012). ER stress preconditioning was first introduced in the anti-Thy1 model of mesangioproliferative glomerulonephritis in rats (Inagi et al., 2008). Pretreatment of rats with a sub-nephritogenic dose of an ER stress inducer, such as tunicamycin (TM) or thapsigargin (TG), ameliorated the severity of the disease by an inhibition of ER stress-induced intracellular signaling.

In the present study, a regimen of ER stress preconditioning, accomplished by TM, was established for hepatic I/R injury in rats, and its effectiveness was confirmed by histology, serum biochemical tests, and ultra-structural observations. Its correlation with IRE1 phosphorylation was noted. In an effort to elucidate its mechanism, receptor for activated C kinase 1 (RACK1), and active AMPK were identified as IRE1 binders in a regulated manner in response to ER stress. The role of RACK1 in ER stress preconditioning of hepatocyte L02 cells was demonstrated by using TM and TG. Surprisingly, BCL2 was phosphorylated by IRE1 at Ser70 by ER stress preconditioning, which exerts hepatoprotection in experimental transplantation.

Results

ER stress preconditioning protects rats from hepatic I/R injury

ER stress is involved in ischemic/hypoxia injury but its mechanistic role in the protective effect of IPC has remained elusive. To determine whether ER stress preconditioning provides hepatoprotection against ischemic/hypoxia injury, we established an animal model in which TM was used to elicit ER stress. By testing different doses and durations of TM treatment in rats, one injection of 100 μg/kg body weight of TM given intraperitoneally at 5 days before I/R injury was found to optimally reduce the serum levels of ALT (alanine aminotransferase) and AST (aspartate aminotransferase) without giving rise to any pathological and ultra-structural changes in the liver (Supplementary Figure S1). To delineate the mechanism of action underlying ER stress in liver, age-matched male Sprague-Dawley rats were divided into five groups and subjected to different doses of TM (50, 100, and 300 μg/kg) and durations of dosing (4, 5, and 6 days). Partial hepatic I/R injury (45 min of ischemia via vascular clamping and 24 h of reperfusion) was accomplished, and the severity of liver damage was determined by measuring serum ALT and AST levels. At the TM dose of 100 μg/kg administered 5 days before the procedure, ER stress preconditioning ameliorated the I/R injury, as determined by reductions in serum ALT and AST levels after 6 and 12 h of reperfusion (Figure 1A and B).

As determined by H&E staining, the pathological changes seen after I/R injury were also alleviated by ER stress preconditioning with TM (Figure 1C). In the I/R group treated with vehicle (saline), a wide range of necrotic hepatocytes and distorted hepatic plates was noted, along with mild expansion of portal and central veins, a large number of infiltrating inflammatory cells, and degeneration (swollen) of hepatocytes. In the I/R group preconditioned with TM, however, no expansion of veins or necrosis of hepatocytes was noted. Only a few swollen hepatocytes with subtle degeneration and a few infiltrating inflammatory cells were found. No fibrosis was noted in any group. The quantitative analysis further supported the above observation (Figure 1D). There was no significant difference in the histological scores between the vehicle sham and TM sham group. Response to I/R treatment, the histological score in the Vehicle I/R group was significantly higher ($P < 0.05$) than in the sham groups, pre-treatment with TM significantly decreased the histological scores compared with the Vehicle I/R group ($P < 0.05$). Western blotting analyses confirmed that no apparent apoptosis was observed in the aforementioned conditions while TM plus I/R resulted in synergistic ER stress response judged by the level of IRE1 phosphorylation at Ser724 (Supplementary Figure S2; top panel, lane 4). Additional analyses using a panel of cell fate markers such as caspase 3, Rip3, and ezrin confirmed that no apparent necrosis was observed in the aforementioned experimental conditions but suggests a possible involvement of autophagic response.

Ultra-structural examination of hepatocytes in different groups was made with transmission electron microscopy (TEM). As shown in Figure 2A, no abnormalities were found in the livers of sham-operated rats dosed with saline. In rats dosed with the ER stress inducer TM and subjected to a sham operation, mitochondrial (annotated with *) density was slightly higher, without obvious abnormalities in ER structure (arrows) and glycogen quantity (Figure 2B). In rats dosed with saline and subjected to I/R injury as shown in Figure 2C, more condensed mitochondria and little glycogen were readily apparent. However, in rats dosed with TM and subjected to I/R injury (Figure 2D), pathological changes were alleviated, in that there was more ER with mild expansion, more glycogen, and more mitochondria with normal density.

To verify the involvement of ER stress in this protective effect, expression of GRP78 was examined as its over-expression was considered as a hallmark of ER stress (Lee, 2005). In addition, phosphorylation of IRE1 has been classified as molecular determinant of ER stress as activation of IRE1 is necessary for GRP78 upregulation (Yoshida et al., 2001). Our preliminary studies showed that the optimal duration of TM treatment in rat is 50 μg/kg for 5 days. Prolong treatment of TM resulted in significant increase in apoptotic cells. Consistent with the notion of ER stress induced by TM treatment, GRP78 was upregulated in response to a typical TM treatment (50 μg/kg for 5 days; Figure 2E). In the I/R groups, with or without ER stress preconditioning, the levels of GRP78 were even higher, suggesting its involvement in ER stress. Similarly, the level of phosphorylated IRE1 was upregulated in the I/R groups and further elevated in rats treated with TM and subjected to I/R. Thus, by inducing UPR, TM treatment provides protection against subsequent hepatic I/R injury, as manifested by increased phosphorylation of IRE1 and elevated GRP78 expression (Figure 2E and G).

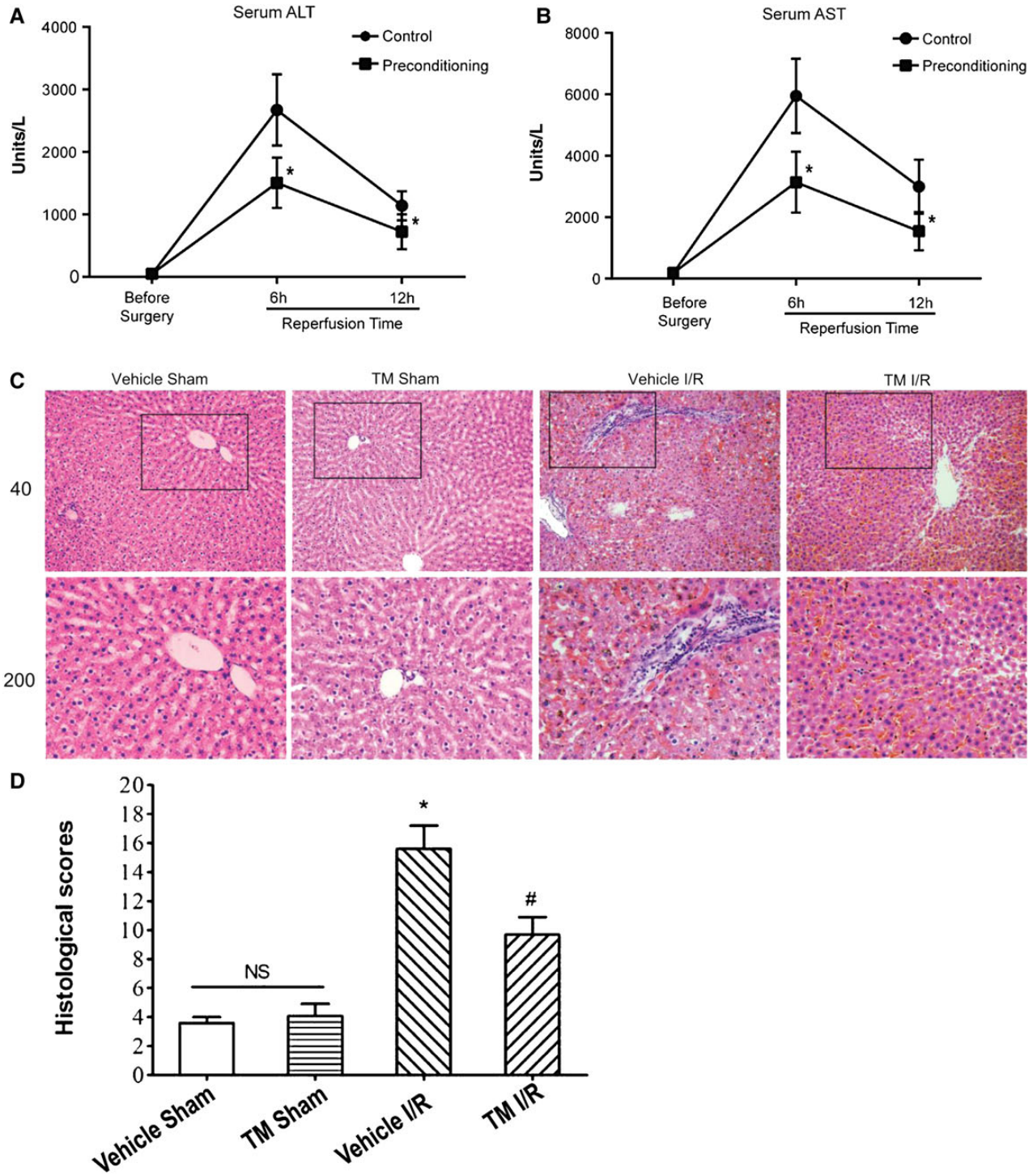

Figure 1 ER stress preconditioning alleviates hepatic I/R injury in rats. (**A** and **B**) Serum ALT/AST levels at different time points after I/R injury with or without ER stress preconditioning (administration of TM, 100 μg/kg body weight at 5 days before surgery). Blood samples were drawn through a tail vein of the rats at indicated time points and prepared for analysis. ALT and AST levels are presented in units/L and expressed as mean ± SD. *$P < 0.05$. (**C**) H&E staining of liver specimens. Representative images of each group are shown. Vehicle Sham, sham-operated group dosed with saline; TM Sham, sham-operated group dosed with TM; Vehicle I/R, partial hepatic I/R group dosed with saline; TM I/R, partial hepatic I/R group dosed with TM (ER stress preconditioning followed by hepatic I/R injury). Liver samples were obtained at 24 h after surgery and prepared for H&E staining. Upper panel, 40× magnification; lower panel, 200× magnification. (**D**) The quantitative analysis of the liver injury scores. H&E staining of liver specimens were assessed for histological scores. Values are expressed as means ± SD. NS, no significant difference. *$P < 0.05$ compared with the sham group; #$P < 0.05$ compared with the I/R group.

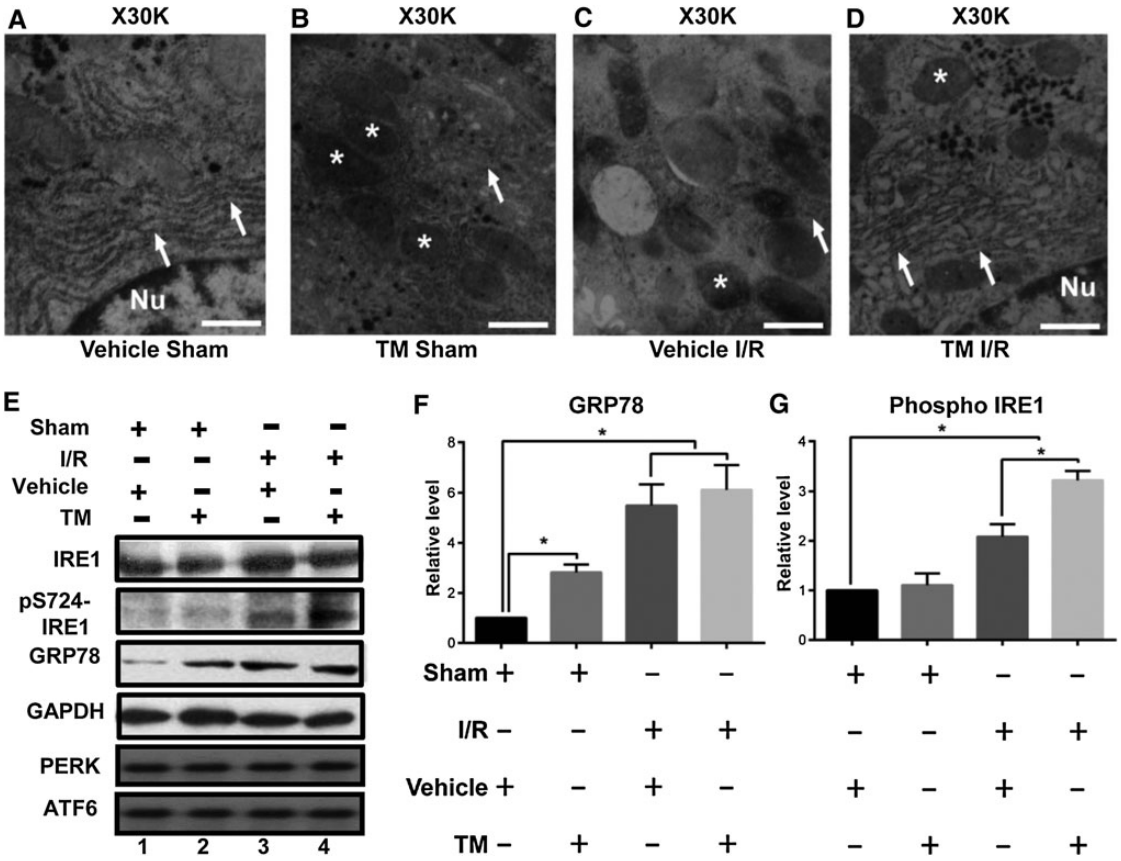

Figure 2 ER stress preconditioning attenuates hepatic ultra-structural damage and elicits IRE1 activation and GRP78 upregulation. (**A**–**D**) Representative TEM images of liver specimens from different dosing groups show subcellular, ultra-structural changes in hepatocytes. Mitochondria are indicated with asterisks, and ER are indicated with arrows. Scale bar, 0.5 μm. (**E**) Representative western blots of IRE1, phosphorylated IRE1 (pS724-IRE1), GRP78, GAPDH, PERK, and ATF6 in liver samples from different dosing groups. (**F** and **G**) Quantification of **E** from three independent experiments. Data are expressed as mean ± SEM. *$P < 0.05$.

Surprisingly, the expression levels of PERK and ATF6 were not altered by either I/R experimentation or TM treatment.

RACK1 and active AMPK interact with IRE1 under ER stress

IRE1 senses the aggregation of misfolded proteins in the ER lumen and elicits the signal by autophosphorylation and subsequent UPR. Under severe and prolonged ER stress conditions, IRE1 is also responsible for the induction of the apoptotic pathway characterized by caspase 12 activation (Wang et al., 1998; Nakagawa et al., 2000). Thus, IRE1 has different roles, in ER stress, depending on the context but its underlying mechanisms have not been elucidated.

To probe the role of IRE1 and its signaling network in ER stress response in HepG2 cells, we carried out immunoprecipitation of HepG2 cells treated with 10 μM TM for 30 min. A representative Coomassie blue-stained gel was presented in Figure 3A. Estimation of molecular weights of co-precipitated polypeptides suggests the possibility of RACK1 and AMPK in the IRE1 precipitates (lane 2). Interestingly, the 35 kDa polypeptide was preferentially retained on the IRE1 affinity matrix from the preparation pretreated with TM. To evaluate whether AMPK and RACK1 interact with IRE1 in a stress-dependent manner, we performed comparative western blotting analyses using TM-treated and DMSO-treated HepG2 cells. As shown in Figure 3B, an increased level of RACK1 was found in IRE1 immunoprecipitates from TM-treated cells as compared with that of control (lane 2). Quantitative analyses revealed that levels of RACK1 and phospho-AMPK are significantly elevated in IRE1 precipitates from TM-treated cells (Figure 3C). To validate whether elevated RACK1 level and phospho-AMPK level are function of ER stress, we also employed TG treatment to induce ER stress. As shown in Supplementary Figure S3A and B, levels of RACK1 and pT172-AMPK were also significantly elevated in IRE1 precipitates from TG-treated cells.

To validate whether phosphorylation of AMPK results from IRE1 activation by TM treatment, we carried out experiments in which HepG2 cells were pretreated with IRE1 inhibitor 4μ8C (10 μM for 30 min) followed by TM treatment. As shown in Figure 3D and E, 4μ8C treatment attenuated the AMPK phosphorylation elicited by TM treatment. The same effect was also observed in L02 cells (Figure 3F). Thus, we conclude that ER stress elicits an IRE1 complex containing abundant RACK1 and active AMPK.

The N-terminal part of IRE1 is in the ER lumen, which senses the accumulation of misfolded proteins while the C-terminal part of IRE1 consists of a phosphorylation and an endonuclease

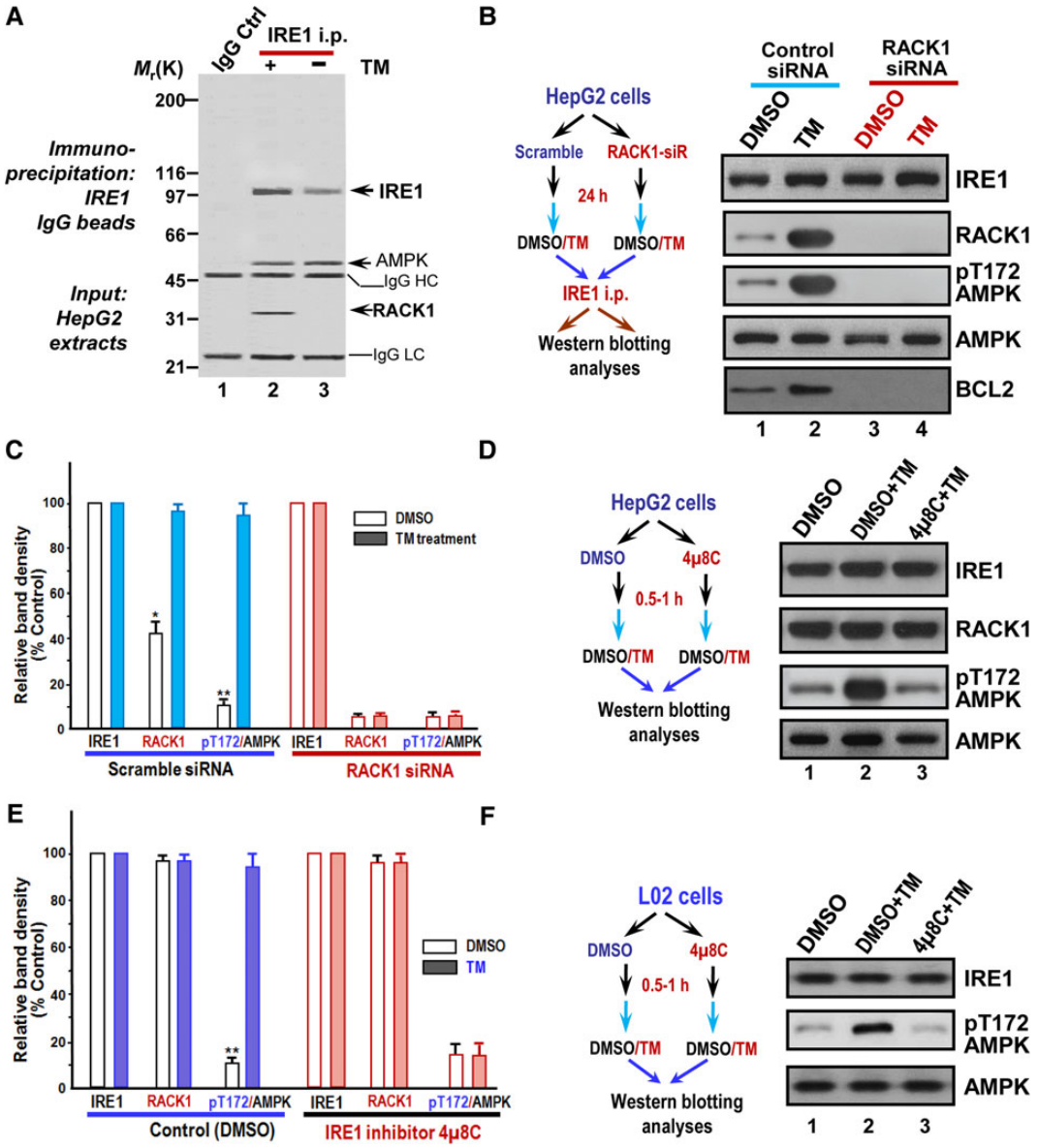

Figure 3 RACK1 forms a complex with IRE1 and AMPK in response to ER stress. (**A**) Co-immunoprecipitation shows that RACK1 forms a complex with IRE1 in HepG2 cells. Aliquots of HepG2 cells were treated with DMSO or TM (15 μM for 30 min) followed by preparation of cell lysates. Clarified cells lysates were incubated with affinity matrix covalently coupled with IRE1 antibodies. A control experiment was performed using Sepharose beads immunobilized with non-specific IgG. A representative Coomassie Blue-stained gel was shown. (**B**) RACK1 orchestrates IRE1 complex containing phosphorylated AMPK in TM-treated HepG2 cells. Aliquots of HepG2 cells were treated with RACK1 siRNA and its scramble control followed by TM treatment. Immunoprecipitation was performed as **A** for HepG2 cells treated with TM and DMSO followed by western blotting analyses. Note that increased amount of RACK1 is presented in IRE1 immunoprecipitates treated with TM compared with DMSO-treated cells, and suppression of RACK1 by siRNA suppresses AMPK phosphorylation. In addition, AMPK in TM-treated group is active based on blotting with pThr172 antibody. (**C**) Quantification of **B** from three independent experiments. Data are expressed as mean ± SD. $^{*}P < 0.05$; $^{**}P < 0.01$. (**D**) Inhibition of IRE1 attenuates TM-elicited AMPK phosphorylation in HepG2 cells. Aliquots of HepG2 cells were pretreated with IRE1 inhibitor 4μ8C (10 μM for 30 min) followed by TM treatment. The treated cells were harvested and analyzed by western blot. Note that AMPK phosphorylation is a function of IRE1 in response to TM treatment. (**E**) Quantification of **D** from three independent experiments. Data are expressed as mean ± SD. $^{**}P < 0.01$. (**F**) Inhibition of IRE1 attenuates TM-elicited AMPK phosphorylation in L02 cells. Aliquots of L02 cells were treated with IRE1 inhibitor 4μ8C followed by TM treatment. The treated cells were harvested and analyzed by western blot. Note that AMPK phosphorylation is a function of IRE1 in response to TM treatment in L02 cells.

domain, and is thus responsible for downstream signals (Iwawaki et al., 2001). Our initial yeast two-hybrid assay indicates that the C-terminal IRE1 directly interacts with RACK1, which was confirmed by the pull-down assay (Supplementary Figure S4). Thus, we conclude that RACK1 interacts with IRE1 under the ER stress condition.

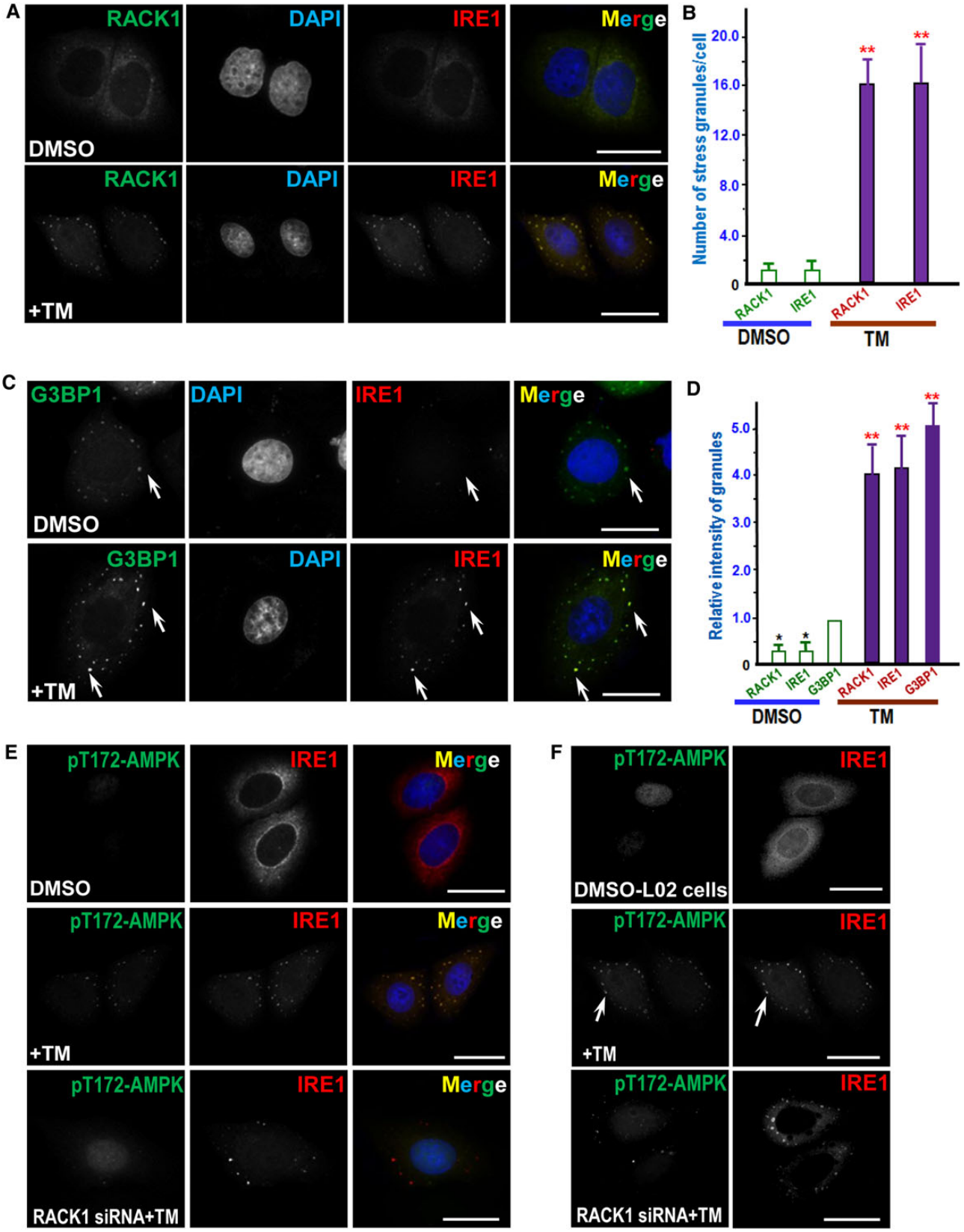

Figure 4 ER stress induced by TM treatment results in a RACK1-dependent co-localization of AMPK with IRE1. (**A**) Immunofluorescence of HepG2 cells probed for IRE1 and RACK1. TM-treated and control cells were fixed and permeabilized as described in Materials and methods, followed by probing with mouse IRE1 antibody and rabbit RACK1 antibody. IRE1 is visualized with a rhodamine-conjugated secondary antibody, while RACK1 is

ER stress elicits a spatial reorganization of IRE1 complex containing active AMPK

We next examined the subcellular localization of IRE1 relative to RACK1 in control and TM-treated HepG2 cells. As shown in Figure 4A, compared with DMSO treatment (upper panel), both IRE1 and RACK1 appear as puncture stress granule-like staining after TM treatment (lower panel), suggesting stress signaling induced dynamic changes of IRE1 and RACK1 distribution. Quantitative analyses show that TM treatment dramatically increased the number of spots per cell positive for RACK1 and IRE1, respectively (Figure 4B). To validate whether IRE1 distributes to stress granule structure in response to TM treatment, we carried out triple immunofluorescence analyses using stress granule marker G3BP1 as previously described (Hou et al., 2011). As shown in Figure 4C, the distribution of IRE1 is superimposed onto that of G3BP1 signal in TM-treated cells (merge; lower panel), confirming the localization of IRE1 to the stress granules in response to TM treatment. Quantitative analyses show that TM treatment dramatically promoted the recruitment of IRE1 and RACK1 to assemble onto G3BP1 positive granules (Figure 4D). Since AMPK presented in IRE1 immunoprecipitates, we then tested the distribution pattern of AMPK relative to IRE1 in control and TM-treated cells. As shown in Figure 4E, TM treatment elicits stress granule-like distribution of pT172-AMPK (middle panel). Significantly, the distribution of pT172-AMPK is attenuated when RACK1 protein level is suppressed (bottom panel), suggesting that RACK1 may function as a signaling scaffold protein during TM-elicited stress response.

To test whether this TM-elicited response is conserved in primary liver cells and whether RACK1 functions as a scaffold protein in other cells, we have carried out similar study using L02 cells. As shown in Figure 4F, there was little staining of pT172-AMPK in control DMSO-treated L02 cells (top panel). However, TM treatment elicits stress granule-like distribution of pT172-AMPK which is reminiscent of IRE1 distribution (middle panel; arrow). Significantly, the distribution of pT172-AMPK is abolished when RACK1 protein level is suppressed by siRNA-mediated knockdown while IRE1 distribution remained apparent in stress granules (bottom panel), indicating that RACK1 may function as a signaling scaffold protein during TM-elicited stress response. Consistent with ER stress-elicited IRE1–RACK1 signaling, TG treatment resulted in similar dynamics of phosphorylation of IRE1 and AMPK associated with stress granules (Supplementary Figure S5). Thus, we conclude that ER stress elicits a spatial reorganization of IRE1 complex containing active AMPK via RACK1 scaffolding.

RACK1 is essential in the protective effect of ER stress preconditioning to alleviate H/R injury

Since RACK1 was required for the activation of IRE1 under ER stress, it appeared likely that RACK1 was also essential for the protective effect of ER stress preconditioning. To test this hypothesis, an ER stress preconditioning model was established with L02 cells by addition of TM into the culture medium prior to hypoxia/re-oxygenation (H/R) injury. The apoptotic effects of different concentrations and durations of TM exposure on L02 cells were determined by flow cytometric assays. The results showed that TM at a concentration of 0.25 μM in the culture medium for 48 h before hypoxia (for 4 h) and reoxygenation (for 6 h) induced GRP78 expression (Figure 5A) and reduced the apoptosis caused by the subsequent H/R injury (Figure 5B). This protective effect was abolished by RACK1 depletion (Figure 5B and C). As *XBP-1* splicing is a characteristic of IRE1 activation, levels of the spliced form of *XBP-1* were measured by real-time RT-PCR. The spliced form was down-regulated in cells depleted RACK1, indicating that, in these cells, inhibition of IRE1 activation correlated with increased apoptosis (Figure 5D). Thus, IRE1 activation is involved in the protective effect of ER stress preconditioning against H/R injury in a RACK1-dependent manner.

ER stress preconditioning elicits BCL2 phosphorylation via IRE1

To further examine whether ER stress preconditioning modulates cell survival activity, we carried out western blotting analyses to evaluate the status of BCL2, an anti-apoptotic modulator. As shown in Figure 6A, a typical inhibition of IRE1 by 4μ8C treatment resulted in a brief reduction of IRE1 phosphorylation (82% ± 5% of the control; top panel, lane 3), which induced a comparable suppression of phosphorylated BCL2 (pS70) but not BCL2 protein level (third and fourth panel, lane 3). Thus, IRE1 is responsible for phosphorylation of BCL2 in TM treated cells.

To test whether IRE1 activation-elicited phosphorylation of BCL2 is conserved in primary liver cells, we examined the levels of phosphorylated BCL2 relative to BCL2 protein level in TM-treated L02

marked by a secondary antibody conjugated to FITC. Scale bar, 10 μm. (**B**) Quantitative analyses of stress-induced granules positive for IRE1 and RACK1 as a function of TM treatment. TM-treated and control cells were fixed, stained, and imaged as described in **A**. A total of 50 cells from three preparations were quantified. Error bars represent SEM. $^{**}P < 0.001$ compared with DMSO-treated cells. (**C**) Immunofluorescence of HepG2 cells probed for IRE1 and G3BP1. TM-treated and control cells were fixed and permeabilized followed by probing with mouse IRE1 antibody and rabbit G3BP1 antibody. IRE1 is visualized with a rhodamine-conjugated secondary antibody, while G3BP1 is marked by a secondary antibody conjugated to FITC. Note that punctuate staining appears in TM-treated cells in which IRE1 and G3BP1 signals are super-imposed (yellow). Scale bar, 10 μm. (**D**) Quantitative analyses of stress granule intensity changes in response to TM treatment. TM-treated and control cells were fixed, stained, and imaged as described in **C**. A total of 50 cells from three preparations were quantified. Error bars represent SEM. $^{**}P < 0.001$ compared with DMSO-treated cells. (**E**) Immunofluorescence of HepG2 cells probed for IRE1 and pT172-AMPK. IRE1 is marked by a rhodamine-conjugated secondary antibody, while pT172-AMPK is labeled by a secondary antibody conjugated to FITC. Aliquots of HepG2 cells were treated with RACK1 siRNA followed by TM treatment (bottom panel). Scale bar, 10 μm. (**F**) Immunofluorescence of L02 cells probed for IRE1 and pT172-AMPK. IRE1 is marked by a rhodamine-conjugated secondary antibody while pT172-AMPK is labeled by a secondary antibody conjugated to FITC. Aliquots of L02 cells were treated with RACK1 siRNA followed by TM treatment (bottom panel). Note that punctuate staining appears in TM-treated cells in which IRE1 and pT172-AMPK signals are super-imposed. Scale bar, 10 μm.

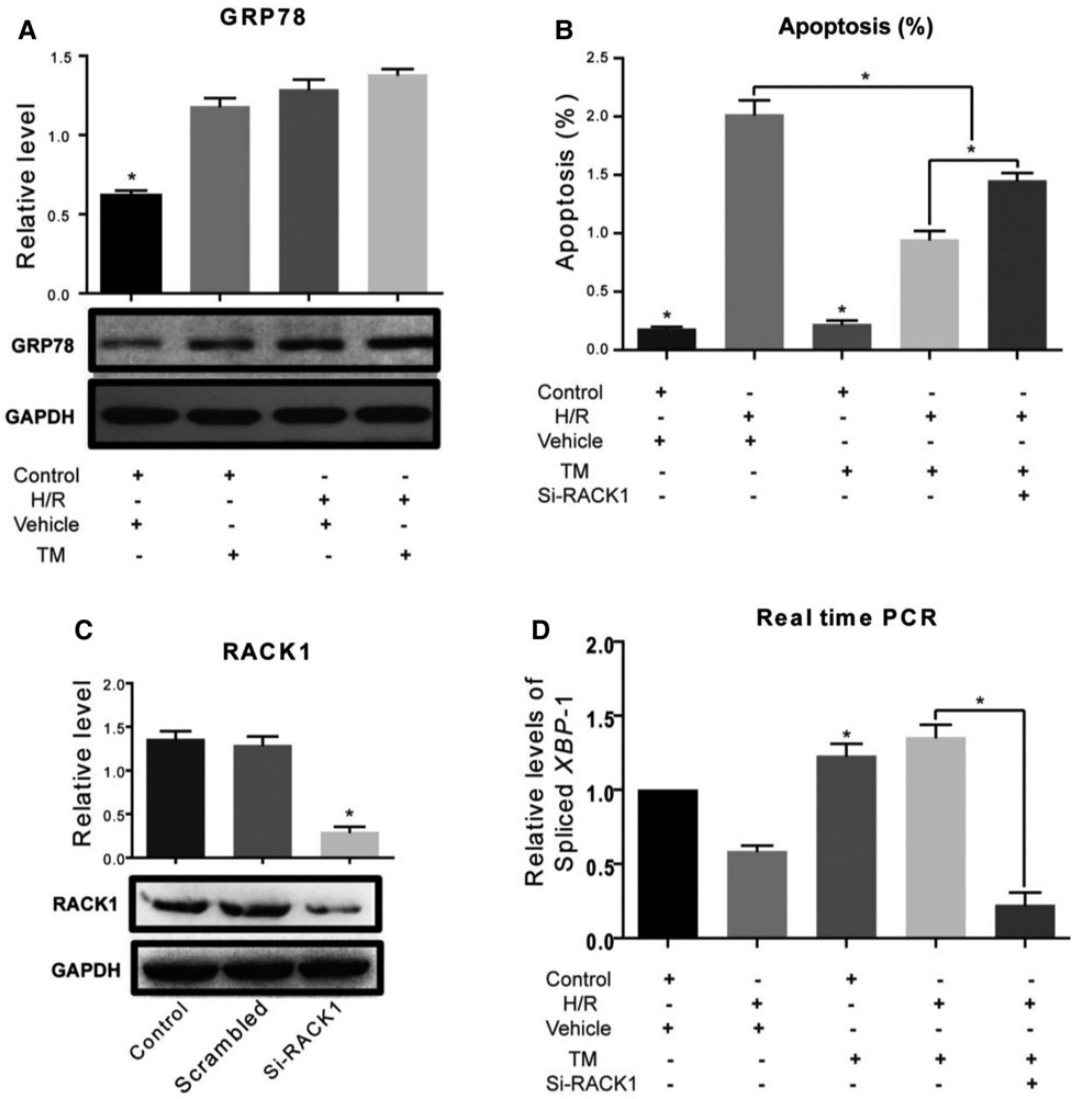

Figure 5 RACK1 is required in ER stress preconditioning to protect cells from H/R injury. (**A**) Western blots of GRP78 in L02 cells after different treatments. Relative levels are expressed as mean ± SD. *$P < 0.05$. Control, cells were cultured in DMEM containing 15% fetal bovine serum at 37°C in 5% CO_2; H/R insult was applied to cells by changing the medium to KHH buffer and incubating in an atmosphere of 2% O_2, 8% CO_2, and 90% N_2 at 37°C for 4 h, followed by re-oxygenation under normal conditions for 6 h. Vehicle, DMSO was used as negative control. TM, cells were exposed to TM (0.20 μg/ml) for 24 h before H/R to achieve ER stress preconditioning. (**B**) Apoptosis rates were determined by flow cytometry. *$P < 0.05$. si-RACK1, cells receiving administration of RACK1 siRNA. (**C**) Western blots of RACK1 in L02 cells show the efficiency of siRNA administration. *$P < 0.05$. Scramble, siRNA of scramble sequence was used as a negative control. (**D**) Relative levels of spliced *XBP-1* mRNA measured by real-time RT-PCR. Results of three individual experiments are shown and expressed as mean ± SD. *$P < 0.05$.

cells. As shown in Figure 6C, phosphorylation of BCL2 at Ser70 and activation of IRE1 judged by phosphorylation of Ser724 are functions of TM treatment (lane 2; middle two panels). Consistent with this observation, pretreatment of IRE1 inhibitor 4μ8C attenuated TM-elicited phosphorylation of BCL2 (lane 3), indicating that IRE1 activation by TM-treatment orchestrates BCL2 phosphorylation.

Recent evidence indicates that phosphorylated BCL2 at serine 70 exhibits great anti-apoptotic functions via regulating autophagy (He et al., 2012). To test whether IRE1 phosphorylates BCL2 at Ser70, FLAG-IRE1 was isolated from HEK293T cells and mixed with hexa-histidine-tagged BCL2 wild type, non-phosphorylatable mutants of S70A and T69A/S84A. As shown in Figure 6D, IRE1 phosphorylates wild type but not mutant BCL2 judged by ^{32}P incorporation (lane 2 and 4). The phosphorylation of S70A mutant BCL2 was greatly suppressed (lane 3). Quantitative analyses show that the level of S70A mutant BCL2 phosphorylation was reduced to 15% ± 5% of the wild type (Figure 6E). Consistent with the general role of BCL2 phosphorylation at Ser70 in ER stress, TG treatment induced elevation of pT172-AMPK and pS70-BCL2 (Supplementary Figure S6A; second to the top panel; lane 2–3). Thus, we conclude that BCL2 is a novel substrate of IRE1, and ER stress preconditioning prevents apoptotic process by phosphorylation of BCL2 via IRE1.

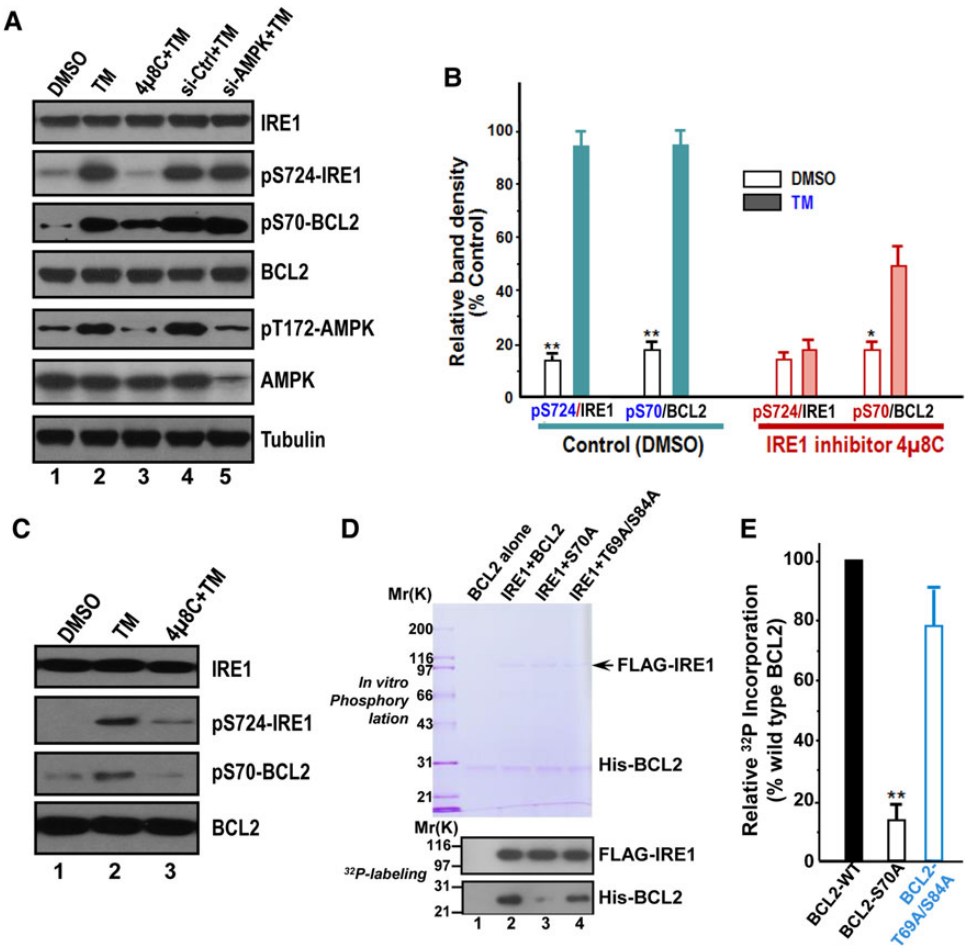

Figure 6 ER stress preconditioning elicits BCL2 phosphorylation at Ser70 via IRE1. (**A**) Western blots of IRE1, phospho-Ser724 IRE1 (pS724-IRE1), phospho-Ser70 BCL2 (pS70-BCL2), BCL2, phospho-Thr172 AMPK (pT172-AMPK), and tubulin in HepG2 cells exposed to treatments as indicated. TM treatment induces phosphorylation of IRE1, AMPK, and BCL2. Note that pS70-BCL2 is a function of IRE1, as inhibition of IRE1 by chemical inhibitor 4μ8C abolished the phosphorylation of BCL2 in response to TM treatment. (**B**) Quantification of **A** from three independent experiments. Data are expressed as mean ± SD. $*P < 0.05$; $**P < 0.01$. (**C**) Western blots of IRE1, pS724-IRE1, pS70-BCL2, and BCL2 in L02 cells exposed to treatments as indicated. TM treatment induces phosphorylation of IRE1 and BCL2. Note that pS70-BCL2 is a function of IRE1, since inhibition of IRE1 by chemical inhibitor 4μ8C abolished the phosphorylation of BCL2 in response to TM treatment as it did in HepG2 cells. (**D**) BCL2 is a substrate of IRE1. Aliquot of recombinant hexa-histidine-tagged BCL2 (wild type and non-phosphorylatable mutants) were incubated with FLAG-IRE1 in the presence of ^{32}P-ATP as detailed in Materials and methods. Upper panel is a representative Coomassie blue-stained gel and lower panel is the autoradiograph of a representative X-ray film. (**E**) Quantification of **D** from three independent phosphorylation experiments. Data are expressed as mean ± SD. $**P < 0.01$.

ER stress preconditioning elicits autophagy via phospho-regulation of BCL2–Beclin 1 interaction

To gain further insight into the BCL2 phosphorylation-mediated survival, we examined the BCL2–Beclin 1 interaction given its role in autophagy regulation. To this end, aliquots of HepG2 cells were treated with IRE1 inhibitor 4μ8C followed by TM treatment. The treated cells were then harvested and subjected to BCL2 immunoprecipitation. The resulting immunoprecipitates were probed for BCL2, pS70-BCL2 and Beclin 1. As shown in Figure 7A, TM treatment resulted in phosphorylation of Ser70 but retained lower level of Beclin 1 compared with the control sample and 4μ8C-treated samples (lanes 1 and 3), indicating that the phosphorylation of BCL2 at Ser70 disrupted the association of BCL2 with Beclin 1.

Recent study showed that BCL2-regulated autophagy contributes to the muscle cell homeostasis (He et al., 2012). To test whether BCL2-regulated autophagy is also involved in TM treatment, we probed LC3 cleavage in response to IRE1 activation. To this end, aliquots of HepG2 cells were treated with IRE1 inhibitor 4μ8C and equal volume of DMSO followed by TM treatment and western blotting analyses of BCL2, pS70-BCL2 and LC3. As shown in Figure 7B, TM treatment elicited autophagy judged by LC3 proteolysis and this proteolytic activity is blocked by IRE1 inhibitor 4μ8C. Thus, we conclude that ER stress preconditioning prevents apoptotic process by activation of autophagy.

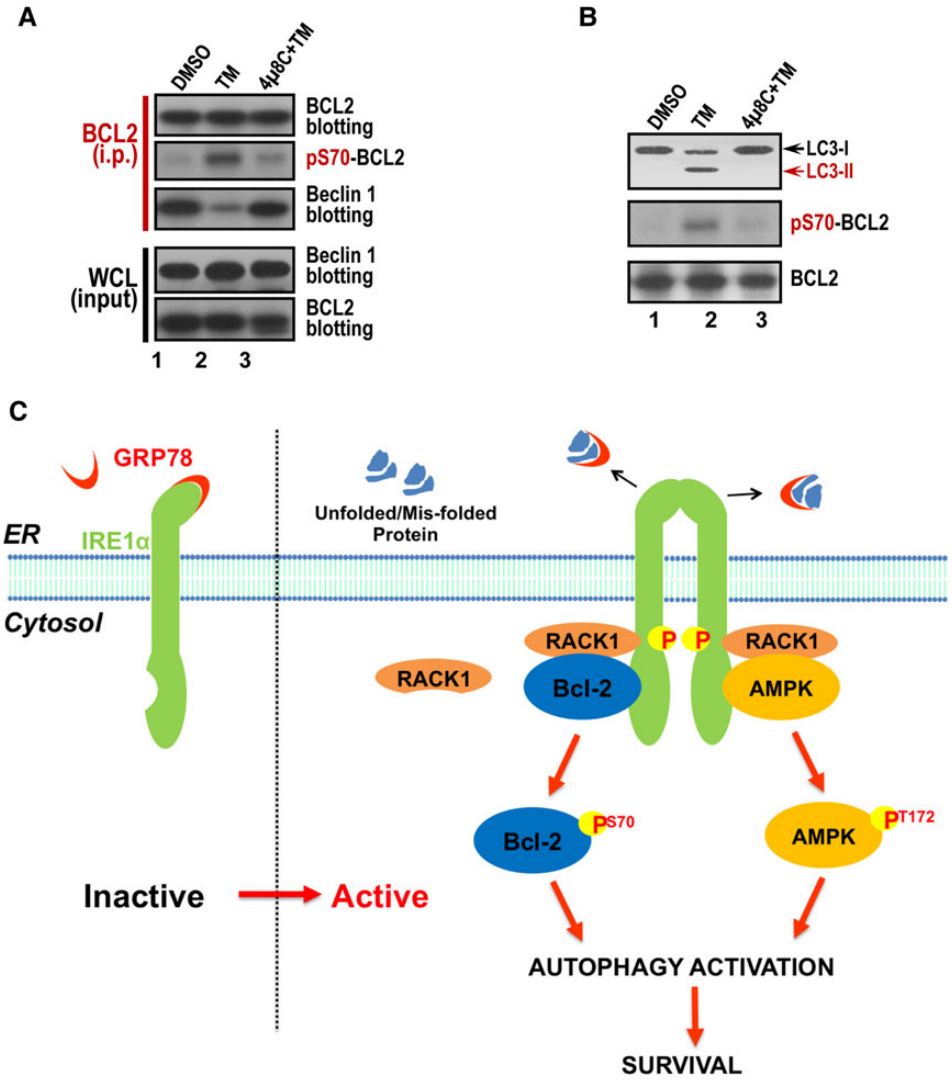

Figure 7 ER stress preconditioning elicits autophagy via phospho-regulation of BCL2–Beclin 1 interaction. (**A**) Phosphorylation of BCL2 perturbs BCL2–Beclin1 interaction. Aliquots of HepG2 cells were treated with IRE1 inhibitor 4μ8C and equal volume of DMSO, followed by TM treatment. The treated cells were harvested and subjected to BCL2 immunoprecipitation. The immunoprecipitates were probed for BCL2, pS70-BCL2, and Beclin 1. Note that phosphorylation of Ser70 releases Beclin 1 from BCL2 binding. (**B**) ER stress preconditioning by TM treatment induces autophagy via LC3 cleavage. Aliquots of HepG2 cells were treated with IRE1 inhibitor 4μ8C and equal volume of DMSO, followed by TM treatment. The treated cells were harvested and subjected to western blotting analyses of BCL2, pS70-BCL2, and LC3. Note that TM treatment elicits autophagy judged by LC3 proteolysis, and this proteolytic event is blocked by IRE1 inhibitor 4μ8C. (**C**) The working model accounting for ER stress preconditioning-elicited cytoprotection from I/R injury. Preconditioning via ER stress elevates AMP/ADP level, which activates AMPK by phosphorylation at Thr172. Phosphorylated AMPK then phosphorylates IRE1 at Ser724. Activated IRE1 further phosphorylates BCL2 at Ser70, which disrupts BCL2–Beclin 1 interaction to trigger autophagy and thus promote cell survival activity.

Discussion

Our findings demonstrate that IRE1–RACK1–AMPK axis is a potent hepatoprotection against ischemia via the activation of BCL2 based on cellular assays and animal model studies. These beneficial hepatoprotective effects of IPC are phosphorylation of BCL2 at Ser70 via IRE1. Thus, BCL2 has previously uncharacterized essential roles in the hepatoprotection against H/R injury. We propose that BCL2-regulated autophagy activation contributes to the beneficial cytoprotective effects of IPC, and that manipulation of the autophagy pathway and/or the function of the autophagy inhibitory BCL2 protein may be a logical strategy to promote the efficiency of liver transplantation.

IRE1 is the most characterized ER resident transmembrane protein and involved in its diversified functions in ER stress (Korennykh et al., 2009). For cells under prolonged ER stress, IRE1 signaling is suppressed in that its clusters are dissociated and its kinase and endoribonuclease activities are inhibited (Li et al., 2010). Thus, it is reasonable to speculate that, under conditions of ER stress, IRE1 activation has a protective effect in the UPR. It would be excited to delineate how IRE1–RACK1–AMPK axis orchestrates hepatoprotective effects.

The interaction between IRE1 and RACK1 also occurs in pancreatic β cells (Qiu et al., 2010). In these cells, IRE1, RACK1, and PP2A form a heterotrimeric complex. Chronic hyperglycemia or ER stress induces the dissociation of PP2A from the complex, which leads to the activation of IRE1 through its autophosphorylation. This finding is consistent with the present observation that RACK1 is required for IRE1 activation under ER stress conditions. This interaction could be the basis of the protective role of ER stress preconditioning. It is interesting to note that the ER stress elicited by TM in liver cell lines did not involve in activation ATF6 and PERK (unpublished data). Although IRE1, PERK and ATF6 all involve in the unfolded protein response, the transgenic knockout studies have demonstrated that IRE1 but not PERK or ATF6 is essential for embryonic viability (Iwawaki et al., 2009; Oslowski and Urano, 2011). It would be of great interest to examine whether there is context-oriented selectivity over the aforementioned three pathways in ER stress response.

Preconditioning is an effective way of protecting the liver and other organs against I/R injury, which is common during surgical procedures such as partial hepatectomy and liver transplantation (Malhi and Gores, 2008). Efforts to elucidate the mechanism of preconditioning are aimed at discovering potential pharmacological interventions that provide more protection and cause less harmful side effects (Tejima et al., 2004; Hart et al., 2008). The present results demonstrate that ER stress preconditioning reduces hepatic I/R injury, which provides a potential alternative to IPC. More work is required to delineate the molecular network underlying hepatoprotection and to translate the essence of IRE1–RACK1–AMPK signaling axis information for minimizing I/R injury in liver transplantation. Our study present here indicates that ER stress preconditioning prevents the apoptotic process by phosphorylation of BCL2 via IRE1 kinase (Figure 7C).

In summary, we demonstrate that ER stress preconditioning induces an interaction of IRE1 with RACK1, which may serve as an interacting hub for signaling molecules such as AMPK. Active AMPK kinase further phosphorylates IRE1 in a spatially regulated pattern. Activated IRE1 phosphorylates BCL2 to exert anti-apoptotic and hepatoprotective effects, providing mechanistic insight into a better understanding of spatiotemporal dynamics underlying ER stress preconditioning. Our findings provide novel insights for better understanding of the molecular pathway underlying ER stress preconditioning-elicited cytoprotective effect against hepatic I/R injury.

Materials and methods

Animals and ethics statements

All animals received humane care according to the criteria outlined in the 'Guide for the Care and use of Laboratory Animals' prepared by the National Academy of Sciences and published by the National Institutes of Health (NIH publication 86–23 revised 1985). Male Sprague Dawley rats (180–220 g, $n = 34$) were purchased from the Animal Center of Fourth Military Medical University and were raised in a clean environment. Surgery procedures were manipulated with care to reduce suffering of the rats during the experiments.

ER stress preconditioning and partial hepatic I/R injury in rats

ER stress preconditioning was induced by intraperitoneal injection of TM (Sigma; T7765) several days before I/R injury. Partial hepatic I/R injury was performed as described (Yu et al., 2011). Blood samples were collected from a tail vein. Serum levels of aspartate aminotransferase (AST) and alanine aminotransferase (ALT) were measured with an automatic biochemical analyzer (HITACHI 7180). Rat livers were collected at 24 h after surgery and prepared for hematoxylin and eosin (H&E) staining as described (Yang et al., 2011). The hepatic damage was evaluated with a Histopathological scoring system according to the previously described methods (Tang et al., 2007). The histological scores is reported as the sum of the individual scores from 0 (no findings) to 1 (mild), 2 (moderate), and 3 (severe) determined by the following six parameters: cytoplasmic color fading, vacuolization, nuclear condensation, nuclear fragmentation, nuclear fading, and erythrocyte stasis.

Transmission electron microscopy

Liver samples were collected at 24 h after surgery and fixed using 2.5% (*v*/*v*) glutaraldehyde in PBS for transmission electron microscopic analyses as previously described (Ding et al., 2010). The samples were post-fixed using osmium tetroxide and cut into ultrathin sections before being photographed using a Hitachi H-7500 TEM.

Western blot

After various treatments, protein samples were subjected to the SDS-polyacrylamide gel, transferred onto nitrocellulose membrane, and probed with following antibodies, respectively: anti-IRE1 (ab37073 for rabbit antibody and ab54692 for mouse antibody, abcam), anti-RACK1 (sc-17754 for mouse antibody, Santa Cruz; ab72483 for rabbit antibody, abcam), anti-phospho-IRE1 Ser724 (ab104157, abcam), anti-GRP78 (sc-13968, Santa Cruz), anti-G3BP1 (ab48739, abcam), GFP (sc-9996, Santa Cruz), anti-GAPDH (SAB1405848, Sigma), anti-phospho-BCL2 Ser70 antibody (2827; CST), anti-BCL2 antibody (2870; CST), anti-AMPK (5832; CST), anti-phospho-AMPK Thr172 (2535; CST) and anti-tubulin antibody (DM1A; Sigma). The signals from western blot were quantified by densitometry and the statistical analyses were conducted from three independent experiments.

Immunoprecipitation

HepG2 cells were treated with 10 μM TM (or 15 μM TG) or equal volume of DMSO for 30 min and then solubilized in lysis buffer (50 mM HEPES, pH7.4, 150 mM NaCl, 2 mM EGTA, 0.1% Triton X-100, 1 mM phenylmethylsulphonyl fluoride, 10 μg/ml leupeptin and 10 μg/ml pepstatin A). Lysates were clarified by centrifugation at 16000 *g* for 10 min at 4°C. Soluble proteins from HepG2 cells were incubated with an anti-IRE1 antibody (ab37073; abcam) covalently coupled to protein-A/G beads (Pierce Chemical) as previously described (Huang et al., 2012). Beads were washed five times with lysis buffer and then boiled in SDS-PAGE sample buffer for 2 min. After SDS-PAGE, proteins were transferred to a nitrocellulose membrane. The nitrocellulose was divided into four strips and incubated with antibodies against IRE1, RACK1, AMPK and pT172-AMPK, respectively, and then with appropriate secondary antibodies. The western blots were visualized using ECL.

Deconvolution microscopy

For immunofluorescence, HepG2 cells were seeded onto sterile, acid-treated 18-mm coverslips. Two hours after replanting, HepG2 cells were treated with 10 μM TM (or 15 μM TG) for 30 min followed by fixation in 4% formaldehyde for 10 min. After rinsed three times in PBS, the coverslips were blocked with 0.05% Tween-20 in PBS (TPBS) with 1% BSA (Sigma). Cells were incubated with various primary antibodies in a humidified chamber for 1 h and then washed three times in TPBS. RACK1 was then visualized using rhodamine-conjugated secondary IgG, and binding of anti-IRE1/pT172-AMPK antibody was visualized using fluorescein-conjugated IgG. DNA was stained with DAPI (Sigma).

Images were collected using a DeltaVision wide field deconvolution microscope system built on an Olympus IX-71 inverted microscope base. For imaging, a 60×/1.42 NA oil lens was used. Images for display were generated by projecting single optical sections as described previously (Yao et al., 2000; Ding et al., 2010).

Cell culture and siRNA transfection

HepG2 cells were purchased from American Tissue Culture Collection, while L02 cells were generous gift from Dr Chaojun Li of Nanjing University. Both were cultured in Dulbecco's modified Eagle's growth medium (DMEM, Invitrogen) containing 15% fetal bovine serum (Hyclone), 100 units/ml penicillin and 100 μg/ml streptomycin (Invitrogen). SiRNAs used in the current study were RACK1 siRNA (sc-36354), IRE1 siRNA oligonucleotide duplexes (sc-40705). Aliquots of L02 cells, or HepG2 cells grown to 40% confluence on 100-mm^2 culture flasks were transfected with Lipofectamine2000 (Invitrogen) premixed with siRNA or a scramble sequence.

ER stress preconditioning of liver cell cultures

Hypoxia injury was applied to L02 cells by changing the medium to Krebs-Henseleit-HEPES (KHH) buffer containing 118 mM NaCl, 4.7 mM KCl, 1.2 mM KH_2PO_4, 1.3 mM $CaCl_2$, 25 mM $NaHCO_3$, and 20 mM HEPES (at pH7.4) and incubating in a hypoxic incubator for 4 h in an atmosphere of 2% O_2, 8% CO_2, and 90% N_2 at 37°C, followed by re-oxygenation in normal complete medium at 37°C in 5% CO_2 for 6 h. Cells were incubated in normal complete medium containing 0.20 μg/ml of TM for 24 h before H/R injury to achieve ER stress preconditioning. Control cells were in a medium containing the same concentration of DMSO.

Annexin V/propidium iodide assays for apoptosis

For Annexin V/PI assays, L02 cells were stained with Annexin V-FITC and PI, and evaluated for apoptosis by flow cytometry according to the manufacturer's protocol (BD Biosciences). The cells were analyzed using a flow cytometer (Calibur™) and the CellQuest software (BD Biosciences). Both early apoptotic (annexin V-positive, PI-negative) and late (annexin V-positive and PI-positive) apoptotic cells were included in cell death determinations.

Real-time polymerase chain reaction

To amplify the spliced form of human *XBP-1*, the primers were 5′-GATTCTGGCGGTATTGACTCTT and AACTGGGTCCTTCTGGGTAG AC-3′. For GAPDH, an internal control, the primers were 5′-GCAC CGTCAAGGCTGAGAAC and TGGTGAAGACGCCAGTGGA-3′. In the thermal cycle reaction, the ABI prism 7500 sequence detection system was used at 50°C for 2 min and 95°C for 10 min, followed by 40 cycles at 95°C for 15 sec and 60°C for 1 min.

Immunoprecipitation of IRE1

The IRE1 complex was isolated from HepG2 cells using an anti-IRE1 mouse monoclonal antibody (3D1; Abnova) coupled to Protein G sepharose as described previously (Yao et al., 1997). Briefly, HepG2 cells were treated with 10 μM TM (or 15 μM TG) for 30 min followed by solubilization with 0.2% NP-40, 50 mM Tris-Cl (pH7.4), 150 mM NaCl, 5 mM EDTA, and proteinase inhibitor cocktail (Sigma). After clarifying the cell lysate, the soluble fraction of lysates was incubated with IRE1 antibody affinity matrix for 2 h at 4°C. After incubation, the beads were washed four times with wash buffer and once with PBS. Samples were resolved by 5%–15% gradient gel and transferred onto nitrocellulose membrane to perform western blotting analyses. Coomassie blue-stained bands were removed for in-gel digestion followed by mass spectrometric identification as described previously (Fang et al., 2006). Positive hits were validated using specific antibodies.

To examine the proteins preferentially associated with IRE1 in an ER stress-induced manner, aliquots of HepG2 cells treated with 10 μM TM or equal volume of DMSO were lysed followed by immunoprecipitation outlined above. Immunoprecipitates from two groups were fractionated by SDS-PAGE followed by western blotting analyses.

Phosphorylation of BCL2 by IRE1 in vitro

Both the hexa-histidine-tagged BCL2 wild type and mutants (S70A; T69A/S84A) proteins were expressed in Escherichia coli BL21 (pLys), and the purification of the fusion proteins was carried out as previously described (Zhao et al., 2013). The fusion proteins bound to nickel-Sepharose beads were suspended in phosphorylation buffer before use.

To verify whether Ser70 of BCL2 is a substrate for IRE1 kinase, 2 μg of purified hexa-histidine-BCL2 fusion protein, both WT and mutants (S70A; T69A/S84A), were incubated with 0.2 μg FLAG-IRE1 isolated from HEK293T cells in phosphorylation buffer containing 20 mM HEPES, pH7.5, 10 mM $MgCl_2$, 5 mM EGTA, 1 mM DTT, 10 nM ATP, and 5 μCi of [γ-^{32}P]-ATP (PerkinElmer Life Sciences) in a total volume of 30 μl. Kinase reaction was carried out at room temperature for 15 min and terminated by SDS-PAGE sample buffer followed by analyses on 5%–15% gradient SDS-PAGE gel. The gel was stained with Coomassie brilliant blue, dried, and quantified by ImageJ (National Institutes of Health).

Statistics

Statistical analyses were performed with the SPSS 12.0 program. Results were expressed as means ± SD. Comparisons between groups were made by the unpaired Student's *t*-test. $P < 0.05$ was considered statistically significant.

Supplementary material

Supplementary Material is available at *Journal of Molecular Cell Biology* online.

Acknowledgements

The authors are grateful for generous gift of L02 cells from Dr Chaojun Li of Nanjing University.

Funding

This work was supported by grants from the National Natural Science Foundation of China (81070363, 30900497, 31271518, 31471275, 31301121, 31471268, 31501095, and 31320103904), National Institutes of Health (CA164133, DK56292), Anhui Provincial Natural Science Foundation (1508085SMC213), China Postdoctoral Science Foundation (2014M560517). W.Y. is an AGA scholar.

Conflict of interest: none declared.

References

Calfon, M., Zeng, H., Urano, F., et al. (2002). IRE1 couples endoplasmic reticulum load to secretory capacity by processing the XBP-1 mRNA. Nature *415*, 92–96.

Carini, R., and Albano, E. (2003). Recent insights on the mechanisms of liver preconditioning. Gastroenterology *125*, 1480–1491.

Ding, X., Yan, F., Yao, P., et al. (2010). Probing CENP-E function in chromosome dynamics using small molecule inhibitor syntelin. Cell Res. *20*, 1386–1389.

Eisen, A., Fisman, E.Z., Rubenfire, M., et al. (2004). Ischemic preconditioning: nearly two decades of research. A comprehensive review. Atherosclerosis *172*, 201–210.

Fang, Z., Miao, Y., Ding, X., et al. (2006). Proteomic identification and functional characterization of a novel ARF6 GTPase-activating protein, ACAP4. Mol. Cell. Proteomics *5*, 1437–1449.

Harding, H.P., Zhang, Y., and Ron, D. (1999). Protein translation and folding are coupled by an endoplasmic-reticulum-resident kinase. Nature *397*, 271–274.

Hart, M.L., Much, C., Gorzolla, I.C., et al. (2008). Extracellular adenosine production by ecto-5′-nucleotidase protects during murine hepatic ischemic preconditioning. Gastroenterology *135*, 1739–1750.e3.

Hayashi, T., Saito, A., Okuno, S., et al. (2003). Induction of GRP78 by ischemic preconditioning reduces endoplasmic reticulum stress and prevents delayed neuronal cell death. J. Cereb. Blood Flow Metab. *23*, 949–961.

He, C., Bassik, M.C., Moresi, V., et al. (2012). Exercise-induced BCL2-regulated autophagy is required for muscle glucose homeostasis. Nature *481*, 511–515.

Hou, H., Wang, F., Zhang, W., et al. (2011). Structure-functional analyses of CRHSP-24 plasticity and dynamics in oxidative stress response. J. Biol. Chem. *286*, 9623–9635.

Huang, Y., Wang, W., Yao, P., et al. (2012). CENP-E kinesin interacts with SKAP protein to orchestrate accurate chromosome segregation in mitosis. J. Biol. Chem. *287*, 1500–1509.

Inagi, R., Kumagai, T., Nishi, H., et al. (2008). Preconditioning with endoplasmic reticulum stress ameliorates mesangioproliferative glomerulonephritis. J. Am. Soc. Nephrol. *19*, 915–922.

Iwawaki, T., Hosoda, A., Okuda, T., et al. (2001). Translational control by the ER transmembrane kinase/ribonuclease IRE1 under ER stress. Nat. Cell Biol. *3*, 158–164.

Iwawaki, T., Akai, R., Yamanaka, S., et al. (2009). Function of IRE1 alpha in the placenta is essential for placental development and embryonic viability. Proc. Natl Acad. Sci. USA *106*, 16657–16662.

Korennykh, A.V., Egea, P.F., Korostelev, A.A., et al. (2009). The unfolded protein response signals through high-order assembly of Ire1. Nature *457*, 687–693.

Lee, A.S. (2005). The ER chaperone and signaling regulator GRP78/BiP as a monitor of endoplasmic reticulum stress. Methods *35*, 373–381.

Li, H., Korennykh, A.V., Behrman, S.L., et al. (2010). Mammalian endoplasmic reticulum stress sensor IRE1 signals by dynamic clustering. Proc. Natl Acad. Sci. USA *107*, 16113–16118.

Machamer, C.E., Doms, R.W., Bole, D.G., et al. (1990). Heavy chain binding protein recognizes incompletely disulfide-bonded forms of vesicular stomatitis virus G protein. J. Biol. Chem. *265*, 6879–6883.

Mahfoudh-Boussaid, A., Zaouali, M.A., Hadj-Ayed, K., et al. (2012). Ischemic preconditioning reduces endoplasmic reticulum stress and upregulates hypoxia inducible factor-1alpha in ischemic kidney: the role of nitric oxide. J. Biomed. Sci. *19*, 1423-0127.

Malhi, H., and Gores, G.J. (2008). Cellular and molecular mechanisms of liver injury. Gastroenterology *134*, 1641–1654.

McCullough, K.D., Martindale, J.L., Klotz, L.O., et al. (2001). Gadd153 sensitizes cells to endoplasmic reticulum stress by down-regulating Bcl2 and perturbing the cellular redox state. Mol. Cell. Biol. *21*, 1249–1259.

Murry, C.E., Jennings, R.B., and Reimer, K.A. (1991). New insights into potential mechanisms of ischemic preconditioning. Circulation *84*, 442–445.

Nakagawa, T., Zhu, H., Morishima, N., et al. (2000). Caspase-12 mediates endoplasmic-reticulum-specific apoptosis and cytotoxicity by amyloid-beta. Nature *403*, 98–103.

Oslowski, C.M., and Urano, F. (2011). Measuring ER stress and the unfolded protein response using mammalian tissue culture system. Methods Enzymol. *490*, 71–92.

Qiu, Y., Mao, T., Zhang, Y., et al. (2010). A crucial role for RACK1 in the regulation of glucose-stimulated IRE1alpha activation in pancreatic beta cells. Sci. Signal. *3*, 2000514.

Ron, D., and Walter, P. (2007). Signal integration in the endoplasmic reticulum unfolded protein response. Nat. Rev. Mol. Cell Biol. *8*, 519–529.

Schroder, M., and Kaufman, R.J. (2005). ER stress and the unfolded protein response. Mutat. Res. *569*, 29–63.

Shen, J., Chen, X., Hendershot, L., et al. (2002). ER stress regulation of ATF6 localization by dissociation of BiP/GRP78 binding and unmasking of Golgi localization signals. Dev. Cell *3*, 99–111.

Tang, B., Qiao, H., Meng, F., et al. (2007). Glycyrrhizin attenuates endotoxin-induced acute liver injury after partial hepatectomy in rats. Braz. J. Med. Biol. Res. *40*, 1637–1646.

Tejima, K., Arai, M., Ikeda, H., et al. (2004). Ischemic preconditioning protects hepatocytes via reactive oxygen species derived from Kupffer cells in rats. Gastroenterology *127*, 1488–1496.

Wang, X.Z., Harding, H.P., Zhang, Y., et al. (1998). Cloning of mammalian Ire1 reveals diversity in the ER stress responses. EMBO J. *17*, 5708–5717.

Yang, J., Zheng, J., Wu, L., et al. (2011). NDRG2 ameliorates hepatic fibrosis by inhibiting the TGF-beta1/Smad pathway and altering the MMP2/TIMP2 ratio in rats. PLoS One *6*, 16.

Yao, X., Anderson, K.L., and Cleveland, D.W. (1997). The microtubule-dependent motor centromere–associated protein E (CENP-E) is an integral component of kinetochore corona fibers that link centromeres to spindle microtubules. J. Cell Biol. *139*, 435–447.

Yao, X., Abrieu, A., Zheng, Y., et al. (2000). CENP-E forms a link between attachment of spindle microtubules to kinetochores and the mitotic checkpoint. Nat. Cell Biol. *2*, 484–491.

Yoshida, H., Matsui, T., Yamamoto, A., et al. (2001). XBP1 mRNA is induced by ATF6 and spliced by IRE1 in response to ER stress to produce a highly active transcription factor. Cell *107*, 881–891.

Yu, H.C., Qin, H.Y., He, F., et al. (2011). Canonical notch pathway protects hepatocytes from ischemia/reperfusion injury in mice by repressing reactive oxygen species production through JAK2/STAT3 signaling. Hepatology *54*, 979–988.

Zhao, X., Wang, D., Liu, X., et al. (2013). Phosphorylation of the Bin, Amphiphysin, and RSV161/167 (BAR) domain of ACAP4 regulates membrane tubulation. Proc. Natl Acad. Sci. USA *110*, 11023–11028.